Atmos. Meas. Tech., 14, 7277–7290, 2021
https://doi.org/10.5194/amt-14-7277-2021

Atmospheric Measurement Techniques
Open Access

Neural-network-based estimation of regional-scale anthropogenic CO_2 emissions using an Orbiting Carbon Observatory-2 (OCO-2) dataset over East and West Asia

Farhan Mustafa[1], **Lingbing Bu**[1], **Qin Wang**[1], **Na Yao**[1], **Muhammad Shahzaman**[2], **Muhammad Bilal**[3], **Rana Waqar Aslam**[4], **and Rashid Iqbal**[5]

[1]Collaborative Innovation Center on Forecast and Evaluation of Meteorological Disasters, Key Laboratory for Aerosol-Cloud-Precipitation of China Meteorological Administration, Key Laboratory of Meteorological Disasters, Ministry of Education, Nanjing University of Information Science and Technology (NUIST), Nanjing 210044, China
[2]School of Atmospheric Sciences (SAS), Nanjing University of Information Science and Technology (NUIST), Nanjing 210044, China
[3]School of Marine Sciences (SMS), Nanjing University of Information Science and Technology (NUIST), Nanjing 210044, China
[4]State Key Laboratory of Information Engineering in Surveying, Mapping and Remote Sensing (LIESMARS), Wuhan University, Wuhan 430079, China
[5]Department of Agronomy, Faculty of Agriculture and Environment, The Islamia University of Bahawalpur, Bahawalpur 63100, Pakistan

Correspondence: Lingbing Bu (lingbingbu@nuist.edu.cn)

Received: 22 July 2021 – Discussion started: 11 August 2021
Revised: 14 October 2021 – Accepted: 15 October 2021 – Published: 18 November 2021

Abstract. Atmospheric carbon dioxide (CO_2) is the most significant greenhouse gas, and its concentration is continuously increasing, mainly as a consequence of anthropogenic activities. Accurate quantification of CO_2 is critical for addressing the global challenge of climate change and for designing mitigation strategies aimed at stabilizing CO_2 emissions. Satellites provide the most effective way to monitor the concentration of CO_2 in the atmosphere. In this study, we utilized the concentration of the column-averaged dry-air mole fraction of CO_2, i.e., XCO_2 retrieved from a CO_2 monitoring satellite, the Orbiting Carbon Observatory-2 (OCO-2), and the net primary productivity (NPP) provided by the Moderate Resolution Imaging Spectroradiometer (MODIS) to estimate the anthropogenic CO_2 emissions using the Generalized Regression Neural Network (GRNN) over East and West Asia. OCO-2 XCO_2, MODIS NPP, and the Open-Data Inventory for Anthropogenic Carbon dioxide (ODIAC) CO_2 emission datasets for a period of 5 years (2015–2019) were used in this study. The annual XCO_2 anomalies were calculated from the OCO-2 retrievals for each year to remove the larger background CO_2 concentrations and seasonal variability. The XCO_2 anomaly, NPP, and ODIAC emission datasets from 2015 to 2018 were then used to train the GRNN model, and, finally, the anthropogenic CO_2 emissions were estimated for 2019 based on the NPP and XCO_2 anomalies derived for the same year. The estimated and the ODIAC CO_2 emissions were compared, and the results showed good agreement in terms of spatial distribution. The CO_2 emissions were estimated separately over East and West Asia. In addition, correlations between the ODIAC emissions and XCO_2 anomalies were also determined separately for East and West Asia, and East Asia exhibited relatively better results. The results showed that satellite-based XCO_2 retrievals can be used to estimate the regional-scale anthropogenic CO_2 emissions, and the accuracy of the results can be enhanced by further improvement of the GRNN model with the addition of more CO_2 emission and concentration datasets.

Published by Copernicus Publications on behalf of the European Geosciences Union.

1 Introduction

Climate change is one of the greatest challenges to the future of Earth, and it stems from global warming, which is accelerated by anthropogenic emissions of greenhouse gases (Lamminpää et al., 2019). The major warming effects are caused by atmospheric CO_2 emissions, and significant amounts of these emissions are contributed by fossil fuel combustion and some industrial activities, such as the calcination of limestone during cement production (Hutchins et al., 2017). The levels of atmospheric CO_2 are continuously increasing (Mustafa et al., 2020), and if these levels continue to increase at the same rate, 1.5 °C of global warming will be reached between 2030 and 2052, which will cause more climate extremes (Hoegh-Guldberg et al., 2021).

Estimates of CO_2 emissions at national, regional, and global levels are now widely reported and have become an important element of public policy and mitigation strategies. Many countries are making efforts to reduce CO_2 emissions. Over the past few decades, significant work has been carried out to compile the regional and the global inventories of CO_2 emissions from anthropogenic activities (Olivier et al., 2005; Janssens-Maenhout et al., 2015; Gurney et al., 2009; Oda and Maksyutov, 2015). Most of the emission inventories employ bottom-up methods using available human activity data, emission factors, and corresponding technologies. The bottom-up methods incorporate energy consumption datasets along with other information, such as fuel purity and efficiency. However, it is known that such information can be subject to errors and biases, leading to considerable discrepancies and uncertainties in emission estimates, especially in the case of rapidly growing developing economies such as China and India (Guan et al., 2012; Korsbakken et al., 2016). These discrepancies can result in ∼40 % to ∼100 % uncertainty in emission estimations at the country and the local scales, respectively (Peylin et al., 2013; Wang et al., 2013). Moreover, defining the uncertainty in the inventory datasets is also a challenging task, and the intercomparisons of various inventories do not necessarily reveal all of the uncertainties, as different inventories sometimes use common sources of information (Konovalov et al., 2016). It is becoming increasingly important to find efficient and reliable ways of monitoring CO_2 reduction progress and to evaluate how well specific CO_2 reduction policies are working.

Satellites provide the most effective way of monitoring atmospheric CO_2 with great spatiotemporal resolution. Several satellites such as the Greenhouse Gases Observing Satellite (GOSAT), GOSAT-2, the Orbiting Carbon Observatory-2 (OCO-2), OCO-3, and TanSAT are orbiting the Earth and are dedicated to monitoring atmospheric CO_2 (Crisp, 2015; Liu et al., 2018; Matsunaga et al., 2019; Taylor et al., 2020; Bao et al., 2020; Hong et al., 2021; Yang et al., 2018). These satellites calculate the average atmospheric CO_2 concentration in the path of sunlight reflected by the surface using spectrometers carried onboard. OCO-2 measures the CO_2 optical depth with bands centered around 1.6 and 2.0 µm and determines the O_2 optical depth using the A-band, which is centered around 0.76 µm (Crisp et al., 2017; O'Dell et al., 2012). The information from these bands is combined to calculate the column-averaged dry-air mole fraction of CO_2 (XCO_2) (Crisp et al., 2012). Several studies suggest that XCO_2 can be used to detect the CO_2 concentration induced by anthropogenic activities by removing the background concentration from the satellite XCO_2 retrievals (Bovensmann et al., 2010; Hakkarainen et al., 2019; Keppel-Aleks et al., 2013). The results from these studies have reported an enhancement of nearly 2 ppm over megacities and high-density urban regions in the US and China. The XCO_2 retrievals derived from the satellite measurements show a positive correlation with the CO_2 emission inventories (Hakkarainen et al., 2016; Yang et al., 2019) which implies that these space-based observations can be used to assess the anthropogenic CO_2 emissions by enhancing the anthropogenic XCO_2 concentration.

Asia is home to the world's most populous nations with the highest CO_2 emissions. East Asia, in particular China, significantly contributes to the global carbon budget and has accounted for ∼ 30 % of the overall growth in global CO_2 emissions over the past 15 years (EDGAR, 2017). This increment in the CO_2 levels is mainly due to the rapid economic growth and anthropogenic activities (Shan et al., 2018). China has pledged to make aggressive efforts to reduce the CO_2 emissions per unit gross domestic product (GDP) by 60 %–65 % relative to 2005 levels, and peak carbon emissions overall, by 2030 (Horowitz, 2016). West Asia is also a region with higher rates of anthropogenic CO_2 emissions (Mustafa et al., 2020), and some of its countries, such as Iran, Saudi Arabia, and Turkey, are listed among the 10 largest CO_2 emitting nations in the world. Several studies have been carried out to estimate the CO_2 emissions using various machine learning techniques, but most of them do not deal with the spatial distribution. Rao (2021) estimated the CO_2 emissions using Support Vector Machine (SVM). Zhonghan et al. (2018) predicted the CO_2 flux emissions based on published data including latitude, age, potential net primary productivity (NPP), and mean depth using the Back Propagation Neural Network (BPNN) and Generalized Regression Neural Network (GRNN) models. Yang et al. (2019) estimated the anthropogenic CO_2 emissions using GOSAT XCO_2 retrievals over China, and the results showed good agreement between the estimated values and the ODIAC CO_2 emission dataset. In this study, we have improved the model initially developed by Yang et al. (2019) to estimate the regional-scale anthropogenic CO_2 emissions using OCO-2 XCO_2 retrievals over East and West Asia. MODIS NPP, OCO-2, and ODIAC CO_2 datasets were obtained for a period of 5 years from January 2015 to December 2019. XCO_2 anomalies were calculated from the OCO-2 retrievals for each year; the GRNN model was trained using XCO_2 anomalies, MODIS NPP, and ODIAC CO_2 emissions with 4 years of data from 2015 to 2018; and then anthropogenic CO_2 emissions were estimated for the year 2019 based on 2019 NPP and XCO_2 anomalies. Atmospheric CO_2 monitoring satellites can detect and analyze the anthropogenic CO_2 signatures, and the satellite-based estimation of anthropogenic CO_2 emissions can be helpful in investigating the carbon emissions as a data-driven method, which is different from the conventional method of calculating an emission inventory. Although the estimation of anthropogenic CO_2 emissions using satellite datasets is a challenging task, as some other factors such as the atmospheric transport and the terrestrial ecosystem play notable roles in controlling the spatial distribution of atmospheric CO_2 (Cao et al., 2017), this data-driven method can still provide meaningful help with respect to quantifying anthropogenic CO_2 emissions that will be important for evaluating the effects of anthropogenic CO_2 emission reduction at regional as well as global scales.

The remainder of this paper is structured as follows: the details of the datasets and methods are provided in Sect. 2, and the results, including the estimated CO_2 emissions, an evaluation of these emissions, and the correlation between ODIAC CO_2 emissions and XCO_2 anomalies are discussed in Sect. 3.

2 Materials and methods

2.1 Datasets

2.1.1 OCO-2 dataset

The Orbiting Carbon Observatory-2 (OCO-2) was launched by the National Aeronautics and Space Administration (NASA) on 2 July 2014 to monitor the concentration of atmospheric CO_2 at regional and global levels (Crisp, 2015). It carries a three-channel imaging grating spectrometer that collects high-resolution, bore-sighted spectra of reflected sunlight. Spectra are collected in the molecular oxygen A-band at 0.765 µm and the CO_2 bands at 1.61 and 2.06 µm (Hakkarainen et al., 2019). Information from all of these bands is combined to calculate the XCO_2. The spatial resolution of OCO-2 is 2.25 km × 1.29 km. More details about the instrument design, calibration approach, in-orbit performance, and measurement principles are provided in a previous study (Crisp, 2015). In this study, we used the OCO-2 Atmospheric Carbon Observations from Space (ACOS)/XCO_2 version 10r product that was generated using the ACOS Level 2 Full Physics (L2FP) retrieval algorithm, which used a Bayesian optimal estimation framework to derive estimates of XCO_2 from spectral measurements of reflected solar radiation (O'Dell et al., 2012; Crisp et al., 2012). A comprehensive study on the validation of OCO-2 XCO_2 retrievals against the Total Carbon Column Observing Network (TCCON) CO_2 dataset reported an absolute median difference of less than 0.4 ppm and a root-mean-square (RMS) difference of less than 1.5 ppm between the two datasets (Wunch et al., 2017). Similar experiments have been carried out for the validation of different versions of OCO-2 XCO_2 products, and the results have shown that the OCO-2 dataset was consistent and reliable for atmospheric CO_2 monitoring (Kiel et al., 2019; O'Dell et al., 2018). The quality and the quantity of the XCO_2 product have been improved with the developments in the ACOS FP retrieval algorithm. The latest OCO-2 XCO_2 product has single sounding precision of ∼ 0.8 ppm over land and ∼ 0.5 ppm over water, and RMS biases of 0.5–0.7 ppm over both land and water (ODell et al., 2021). The evolution of the ACOS L2FP retrieval algorithm from v7 to v10 is summarized in Table 1.

No major changes were made in the ACOS v9 L2FP retrieval algorithm relative to v8 except for the sampling of the meteorological prior. The trace gas absorption coefficient tables (ABSCO) were updated in various versions of the ACOS L2FP retrieval algorithms. The source of the prior meteorology was changed from the European Center for Medium-Range Weather Forecasts (ECMWF) in ACOS v7 to the NASA Goddard Modeling and Assimilation Office (GMAO) Goddard Earth Observing System (GEOS) Forward Processing – Instrument Team (FP-IT) products for v8 and v9. The aerosol prior source was changed from the GMAO Modern-Era Retrospective analysis for Research and Applications (MERRA) product in v7–9 to Goddard Earth Observing System 5 (GEOS5) FP-IT in v10. Moreover, an additional stratospheric aerosol layer was introduced in ACOS v8–10. The prior value of aerosol optical depth (AOD) for each retrieved aerosol type was lowered from 0.0375 in v7 to 0.0125 in v8–10. The CO_2 prior developed by the Total Carbon Column Observing Network (TCCON) team using the ggg2014 algorithm remained same in v7, v8, and v9 of the algorithm. Another major change was switching the land surface model from a purely Lambertian land surface model to a bidirectional reflectance distribution function (BRDF) model (Taylor et al., 2021).

2.1.2 ODIAC dataset

ODIAC is a global emission data product of CO_2 emissions from fossil fuel combustion provided with 1 km × 1 km and 1° × 1° spatial resolutions (Oda, Tomohiro, 2015). It shares country-scale estimates with the Carbon Dioxide Information Analysis Center (CDIAC) but distributes the emissions differently within the countries and includes gridded international bunker emissions (Oda and Maksyutov, 2015). CDIAC distributes the CO_2 emissions based on the population density, whereas ODIAC incorporates power plant profiles and nighttime light observations for emission distribution (Wang et al., 2020). ODIAC shows better agreement with the US bottom-up inventory (Gurney et al., 2009) than CDIAC, and it is commonly used in flux inversions (Crowell et al., 2019; Lauvaux et al., 2016; Maksyutov et al., 2013; Takagi et al., 2011). In this study, we used the 2020 version of ODIAC emission dataset that is freely available and can be down-

Table 1. Evolution of the Atmospheric Carbon Observations from Space (ACOS) Level 2 Full Physics (L2FP) retrieval algorithm (Taylor et al., 2021).

		ACOS v7	ACOS v8/9	ACOS v10
1	Spectroscopy	ABSCO v4.2	ABSCO v5.0	ABSCO v5.1
2	Meteorology prior source	ECMWF	GEOS5 FP-IT	No changes
3	Aerosol prior source	MERRA monthly climatology	No changes	GEOS5 FP-IT with tightened prior uncertainty
4	Retrieved aerosol types	Water, ice, and two MERRA types	With stratospheric aerosol	No changes
5	AOD prior value (per type)	0.0375	0.0125	No changes
6	CO_2 prior source	TCCON ggg2014	No changes	TCCON ggg2020
7	Land surface model	Lambertian	BRDF	No changes

loaded from http://db.cger.nies.go.jp/dataset/ODIAC/ (last access: 3 June 2021).

2.2 Methods

The estimation of anthropogenic CO_2 emissions includes three major steps, as shown in Fig. 1: the first step includes enhancing the XCO_2 concentration influenced by anthropogenic activities; the second step involves setting up the GRNN model using the XCO_2, NPP, and ODIAC datasets; and the final step is the validation of estimated CO_2 emissions against the actual ODIAC emission dataset.

The OCO-2 XCO_2 dataset was downloaded from the EARTHDATA platform (https://earthdata.nasa.gov/, last access: 28 May 2021); to ensure the reliability of the data, screening and filtering of the dataset was carried out following the instructions given in the OCO-2 Data User Guide (DUG). Each sounding that is processed using the ACOS L2FP retrieval algorithm is assigned either a “good” (0) or “bad” (1) quality flag based on screening criteria derived from comparisons with TCCON and modeled CO_2 fields. It is generally advised that users should use the good-quality soundings for regional- and local-scale studies because the soundings flagged as bad-quality might include biases that compromise their utility for the application. In this study, the OCO-2 XCO_2 retrievals were included if (i) they were flagged good (flag of 0) and (ii) the standard deviation of the good soundings for the day was less than 2 ppm. CO_2 has a larger background concentration and a longer atmospheric lifetime than other greenhouse gases (Hakkarainen et al., 2019). Hence, XCO_2 varies by nearly 2 % over the seasonal cycle and from pole to pole. In addition, XCO_2 variations influenced by anthropogenic activities are also smaller on the scale of satellite soundings (2–4 km^2). Therefore, high precision is critical for the accurate quantification of the XCO_2 anomalies related to anthropogenic activities. To highlight the emission areas, CO_2 seasonal variability and the large background concentrations must be removed.

To highlight the areas associated with the anthropogenic CO_2 emission, XCO_2 anomalies were calculated by subtracting the daily XCO_2 median (daily background) from the individual XCO_2 observation – a method suggested by previous studies (Hakkarainen et al., 2019, 2016):

$$XCO_2\ (\text{anomaly}) = XCO_2\ (\text{individual}) - XCO_2\ (\text{daily background}). \quad (1)$$

This equation calculated the XCO_2 anomalies for each observation. Subtraction of the daily background concentration removes the seasonal variability. The space-based soundings are irregularly distributed and have spatiotemporal gaps because a large amount of the satellite observations is removed after screening for clouds and other artifacts. To deal with the spatiotemporal gaps, kriging interpolation was used, and a mapping dataset was generated with a spatial resolution of $0.5° \times 0.5°$ (latitude × longitude) and a temporal resolution of 16 d. Finally, the mean of each grid cell was calculated for each year from 2015 to 2019. The annual mean of XCO_2 (anomaly) can detrend the seasonal variation (Hakkarainen et al., 2016). The annually averaged XCO_2 anomalies were resampled at a grid with a spatial resolution of $1° \times 1°$ (latitude × longitude) and used along with $1° \times 1°$ (latitude × longitude) ODIAC emission dataset to set up the GRNN model.

During the process of photosynthesis, living plants convert CO_2 into sugar molecules that they use for food. In the process of making food, they also release the oxygen we breathe. Plant productivity plays a crucial role in the global carbon cycle by absorbing the CO_2 released by anthropogenic activities. The net primary productivity (NPP) shows how much CO_2 is absorbed by plants during photosynthesis minus how much CO_2 is released during respiration. A negative NPP value means that CO_2 is released into the atmosphere, and a positive value represents the absorption of atmospheric CO_2. To improve the model results, an NPP dataset (MOD17A3HGF) provided by MODIS has also been used in this study. It provides information about annual NPP and is distributed by NASA’s Land Processes Distributed Active Archive Center (LP DAAC). The NPP dataset with a spatial resolution of 500 m was downloaded from the LP DAAC website (https://lpdaac.usgs.gov/products/mod17a3hgfv006/, last access: 2 September 2021). The annual NPP is derived from the sum of all 8 d Net Photosynthesis (PSN) products (MOD17A2H) from the given year. The MODIS NPP dataset was reprojected and resam-

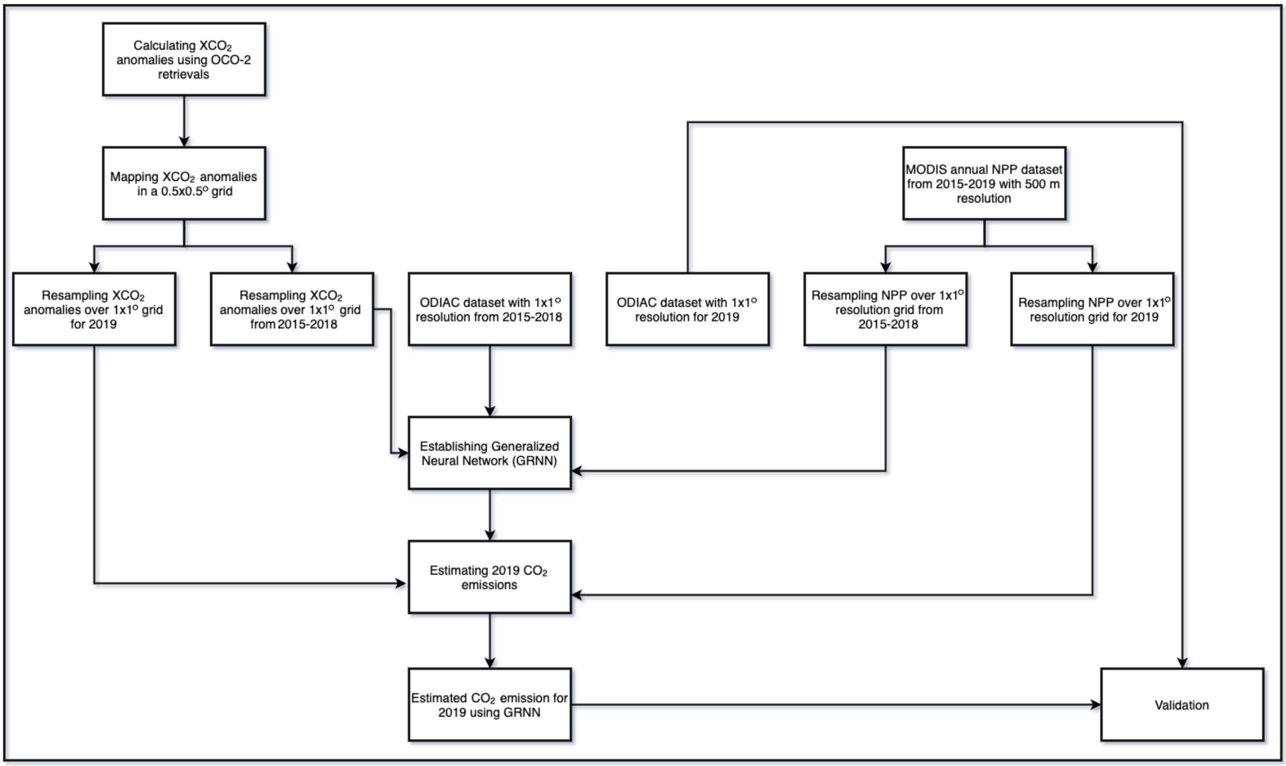

Figure 1. Flowchart explaining the steps involved in estimating the anthropogenic CO_2 emissions using MODIS NPP and OCO-2 XCO_2 retrievals.

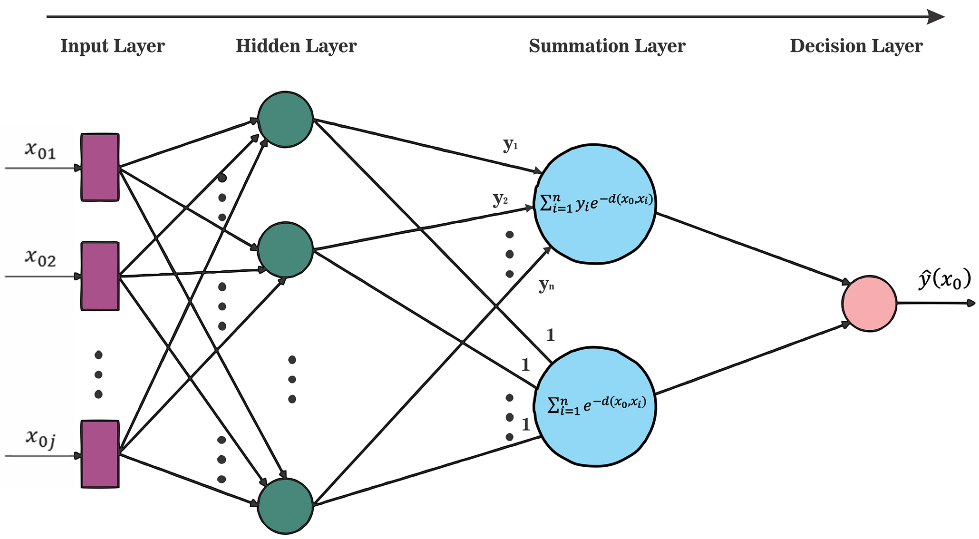

Figure 2. Flowchart explaining the steps involved in estimating the anthropogenic CO_2 emissions using OCO-2 XCO_2 retrievals (Yang et al., 2019).

pled to the spatial resolution of $1° \times 1°$ (latitude × longitude) for each year and used along with the ODIAC and OCO-2 datasets to train the GRNN model and as well predict the CO_2 emissions.

XCO_2 variations are primarily influenced by anthropogenic activities and terrestrial ecosystems, and there is both linear and nonlinear mapping between the XCO_2 and the emissions. We adopted the GRNN algorithm to represent the nonlinear mapping between the independent variables

(XCO_2 anomaly and NPP) and the dependent variable (CO_2 emissions). The GRNN is a memory-based network that provides estimates of continuous variables and converges to an underlying regression. The regression of a dependent variable on an independent variable is the computation of the most probable value of the dependent variable for each value of the independent variable based on a finite number of possibly noisy measurements of the independent variable and the associated values of the dependent variable. The dependent and the independent variables are usually vectors (Rooki, 2016). The architecture of GRNN is shown in Fig. 2. It consists of four layers including an input layer, a hidden layer, a summation layer, and a decision layer. In the input layer, each neuron corresponds to the independent variable that is expressed as a mathematical function, and the independent variable values are standardized. The standardized values of the independent variable are then transferred to the neurons in the hidden layer. In this layer, each neuron stores the values of the dependent and independent variables and calculates a scalar function. The third layer, known as the summation layer, contains two neurons: the denominator summation unit, which sums the weight values being received from the hidden layer, and the numerator summation unit, which sums the weight values multiplied by the actual target-dependent variable value for each hidden neuron. Finally, the target-dependent value is obtained in the decision layer by dividing the value accumulated in the numerator summation unit by the value in the denominator summation unit. To develop a neural network, the dependent and the independent training variables must be standardized so that all training data will have the same order of magnitude in the input layer (Yang et al., 2019).

$$\mathrm{d}(x_0 - x_i) = \sum_{j=1}^{p} \left[\frac{x_{0j} - x_{ij}}{\sigma} \right]^2, \tag{2}$$

where p is the dimension of the variable vector x_i, σ is the spread parameter, and an optimal spread parameter value is obtained after several runs following the mean squared error of the estimated values, which must be kept at a minimum (Rooki, 2016). In this study, values of spread parameters were optimized using the "Holdout Method". More details about the Holdout Method are provided in a previous study (Specht, 1991). The weight of the denominator neuron was set to 1.0. The predicted target dependent variable was defined by the following equation:

$$\hat{y}(x_0) = \frac{\sum_{i=1}^{n} y_i e^{-\mathrm{d}(x_0, x_i)}}{\sum_{i=1}^{n} e^{-\mathrm{d}(x_0, x_i)}}, \tag{3}$$

where the values calculated with the scalar function in a hidden neuron i are weighted with the corresponding values of the training samples y_i. n denotes the number of training samples.

3 Results and discussion

3.1 Spatial distribution of XCO_2 observations and anomalies

The satellite-based observations are sensitive to clouds and aerosols; therefore, many of the data are discarded during preprocessing due to the presence of clouds and aerosols (Mustafa et al., 2021b). Figure 3a and b show the quantity of XCO_2 retrievals from 2015 to 2019 on a spatial grid of $0.5° \times 0.5°$ (latitude × longitude) over West and East Asia, respectively. OCO-2 shows good spatial coverage over East Asia; however, the southern parts of the region, in particular the Tibetan Plateau, have a relatively lower number of XCO_2 retrievals. The Tibetan Plateau is the most extensively elevated surface on Earth, and satellite measurements show larger uncertainties over this region (Yang et al., 2019). In the case of West Asia, the southern parts of the region have a lower number of XCO_2 retrievals. A very large desert, the Rub' al Kahli, is located in this area; it stretches across Saudi Arabia, Yemen, Oman, and the United Arab Emirates (UAE) and often observes dust storms. The lower number of XCO_2 retrievals in these parts of the region might be due to the ACOS XCO_2 retrieval algorithm that excludes satellite measurements with a high aerosol optical depth and cloud optical thickness (Crisp et al., 2012; O'Dell et al., 2012).

Figure 3c shows the spatial distribution of the 5-year averaged XCO_2 anomalies calculated using the method described in Sect. 2.2 over West Asia. The higher concentrations of XCO_2 anomalies were observed over the central parts of the region that included Iran, Kuwait, Saudi Arabia, and Iraq. Iran and Saudi Arabia are listed among the top 10 CO_2 emitting nations and produce over 6 % of the global CO_2 emissions (Jalil, 2014). In addition, Iran, Saudi Arabia, and Iraq are the major fuel consumers of the region and contribute more than 60 % of the region's total fossil fuel CO_2 emissions (Boden et al., 2017). Figure 4d shows the multiyear averaged XCO_2 anomalies over East Asia. The eastern parts of the region including eastern China, Japan, and South Korea show the highest concentrations of XCO_2 anomalies. China's Beijing–Tianjin–Hebei area, Korea, and Japan are the most populated urban regions with high amounts of anthropogenic emissions in the world (Mustafa et al., 2020).

Figure 3e shows the monthly averaged XCO_2 over East and West Asia. The monthly averaged XCO_2 concentrations show seasonal fluctuations. Moreover, the XCO_2 concentrations during each month are higher than those in the same month of the previous year, which reflects that the XCO_2 concentration in the atmosphere is continuously increasing in both regions. The XCO_2 concentration starts increasing from September and reaches its maximum value in April; it then starts decreasing and reaches its minimum value in August. The decrement in its concentration from May to August is due to several reasons; however, it is primarily owing to the strong photosynthesis and weak respiration rate

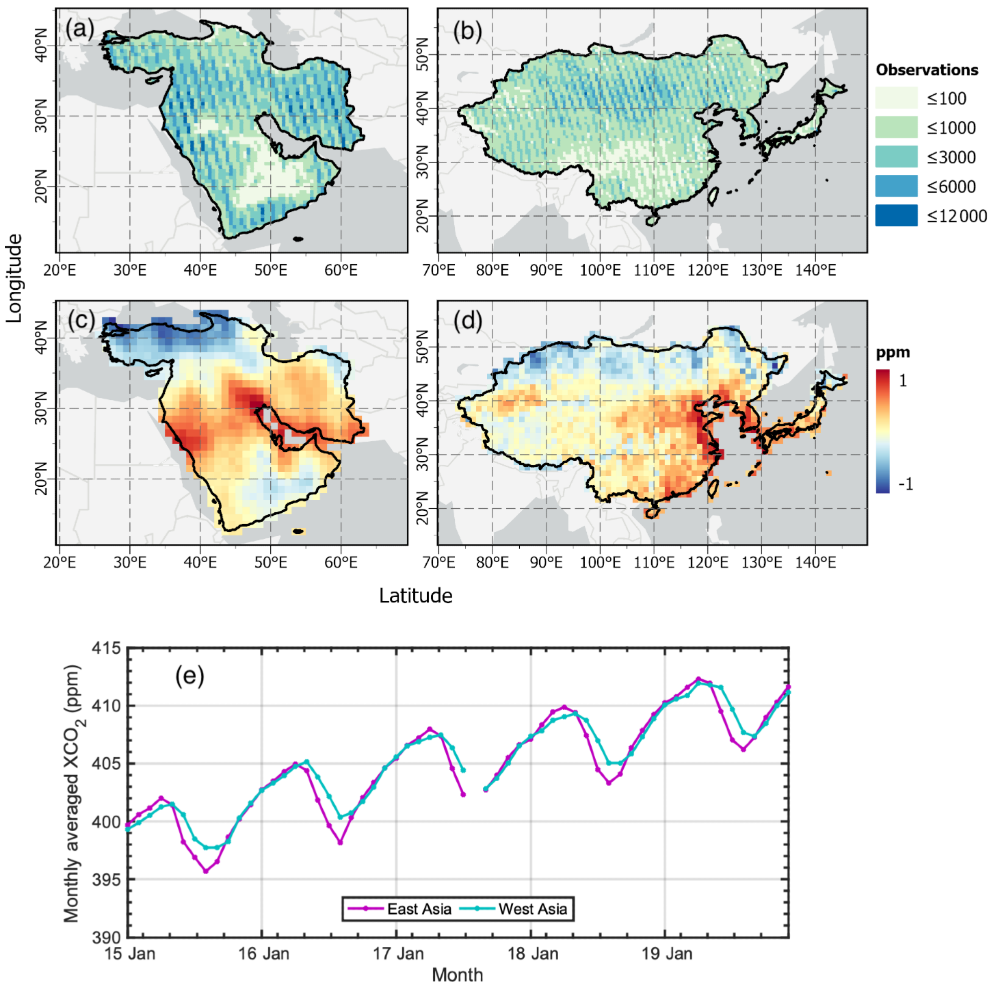

Figure 3. Number of observations in each cell of a $0.5 \times 0.5°$ grid for a period of 5 years from 2015 to 2019 over **(a)** West Asia and **(b)** East Asia; the 5-year mean of XCO_2 anomalies calculated using OCO-2 retrievals over **(c)** West Asia and **(d)** East Asia; and **(e)** the monthly averaged XCO_2 concentration from 2015 to 2019 over East and West Asia. (The base map was sourced from OpenStreetMap.)

of plants, which is enhanced during the monsoon or rainy season (Mustafa et al., 2020). The increment in the XCO_2 concentration from September to April is likely to be caused by weak photosynthesis and strong respiration, the use of heating systems in winter, and strong microbial activity (Cao et al., 2017; Mustafa et al., 2021a).

3.2 Estimated CO_2 emissions

The annually averaged XCO_2 anomalies, MODIS NPP, and ODIAC CO_2 emission datasets for a period of 4 years from 2015 to 2018 were used as a training dataset for the GRNN model built to estimate the CO_2 emissions using the method described in Sect. 2.2. The GRNN model was then applied to 2019 annually averaged XCO_2 anomalies and NPP datasets to predict the CO_2 emissions with the same unit as the ODIAC CO_2 emissions. The analyses were carried out separately over East and West Asia. Figure 4a and b show the estimated values and the ODIAC CO_2 emissions over East Asia, respectively. The results show that the estimated values and the inventory CO_2 emissions exhibit nearly the same spatial distribution pattern. The eastern part of the region shows higher CO_2 emissions, and the western and northern parts, in particular the Tibetan Plateau and Mongolia, show the minimum CO_2 emissions. The pattern is also similar to the XCO_2 anomalies distribution over East Asia (Fig. 3d). The estimated CO_2 emissions have a relatively smoother distribution pattern compared with the ODIAC CO_2 emissions, which might be due to the interpolation of the OCO-2 dataset. Figure 4c shows the difference between the estimated and the inventory CO_2 emissions over East Asia. The estimated CO_2 emissions are generally overestimated relative to the ODIAC CO_2 emissions; however, the emissions are underestimated over some parts of the region as well. Figure 4d shows the land cover distribution of East Asia provided by the Copernicus Global Land Service (Buchhorn et al., 2020). The predicted CO_2 emissions are overestimated

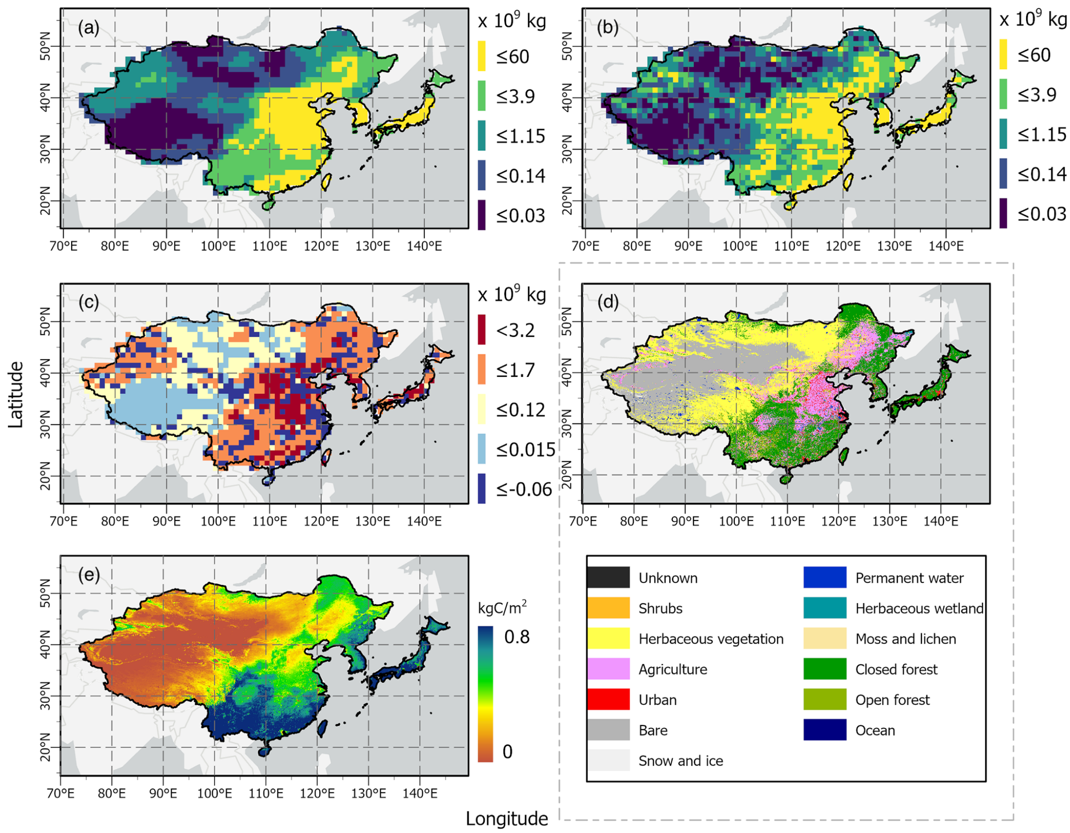

Figure 4. Spatial distribution of **(a)** OCO-2 XCO_2-based anthropogenic CO_2 emission estimates for 2019, **(b)** actual ODIAC emissions for 2019, **(c)** their difference (estimated emission minus actual emission), **(d)** 100 m resolution land cover distribution provided by the Copernicus Global Land Service over East Asia, and **(e)** the spatial distribution of NPP. (The base map was sourced from OpenStreetMap.)

over most of the regional parts; however, this overestimation is more significant over agricultural areas that are located near high-density regions, e.g., eastern China. Eastern China, Japan, and Korea are known to be among the regions with the highest CO_2 emissions, and this underestimation over the agricultural areas might be caused by the nearby CO_2 emission sources which raise the CO_2 concentration of the nearby areas through atmospheric transport. Previous studies have demonstrated that the concentration of atmospheric CO_2 is influenced by atmospheric transport (Cao et al., 2017; Kumar et al., 2014). The areas where the predicted CO_2 emissions are underestimated are covered by agriculture, forest, and vegetation. This underestimation of the predicted CO_2 emissions over these areas indicates the presence of uncertainties in the XCO_2 anomalies that are likely to be produced by the CO_2 uptake of the biosphere which still remains in the XCO_2 anomalies. In addition, the areas where the estimated CO_2 emissions are overestimated have higher elevations. OCO-2 observations show larger uncertainties over elevated and mountainous areas, especially the Tibetan Plateau where the OCO-2 retrievals are significantly overestimated (Kong et al., 2019; Mustafa et al., 2020), and this might also have a contribution to the overestimation of estimated CO_2 emissions. The difference between the estimated and the ODIAC CO_2 emissions ranged from -0.06×10^9 to 3.2×10^9 kg, and the magnitude of difference between -1×10^9 and 1×10^9 kg accounted for 84 % of the total number of grid cells. Yang et al. (2019) estimated the CO_2 emissions using a similar machine learning approach with GOSAT XCO_2 retrievals over China, and the differences between the estimated values and the ODIAC CO_2 emissions were between -5×10^9 and 5×10^9 kg. Moreover, the predicted results from the above-mentioned study exhibited less CO_2 emissions overall relative to the ODIAC emissions, contradicting our results. Our study showed better results, which may be due to the fact that (i) we improved the predictive model with the addition of an NPP dataset (Fig. 4e), (ii) we utilized the higher-resolution XCO_2 retrievals provided by OCO-2, and (iii) we incorporated the OCO-2 XCO_2 retrievals processed using the latest version of the retrieval algorithm. The newer version of the ACOS L2FP retrieval algorithm has improved the quantity and the quality of the satellite-based observations (Taylor et al., 2021).

Figure 5a and b show the spatial distribution of satellite-based estimated CO_2 emissions and the actual ODIAC CO_2 emissions over West Asia, respectively. The spatial distribu-

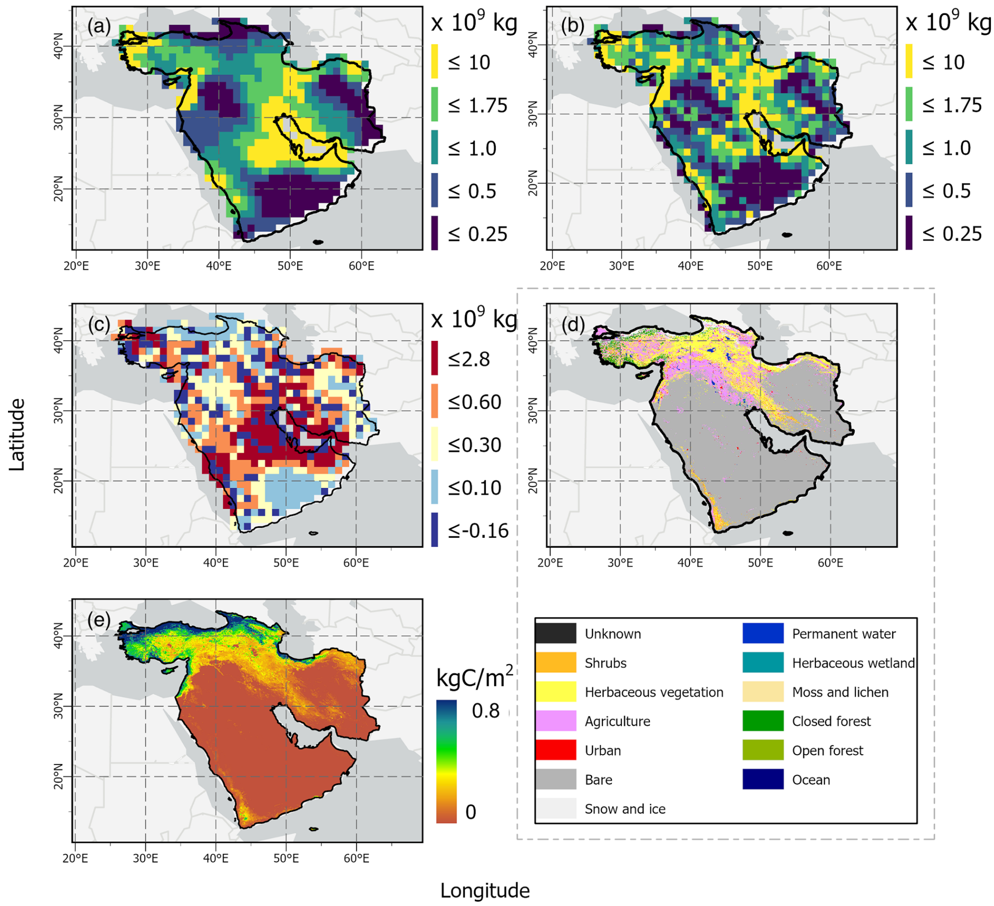

Figure 5. Spatial distribution of **(a)** OCO-2 XCO_2-based anthropogenic CO_2 emission estimates for 2019, **(b)** actual ODIAC emissions for 2019, **(c)** their difference (estimated emission minus actual emission), **(d)** 100 m resolution land cover distribution provided by the Copernicus Global Land Service over West Asia, and **(e)** the spatial distribution of NPP. (The base map was sourced from OpenStreetMap.)

tion pattern of both the estimated and the original CO_2 emissions is similar with some differences in their magnitudes. CO_2 emissions in the eastern parts are relatively larger compared with other parts of the region. Figure 5c shows the difference between the estimated values and the ODIAC CO_2 emissions. The satellite-based estimated CO_2 emissions are generally overestimated compared with the actual ODIAC CO_2 emissions. The estimated CO_2 emissions are notably larger over Iran and Saudi Arabia. Figure 5d shows the land cover distribution of West Asia. It can be seen that the predicted CO_2 emissions are overestimated over the areas that are covered by either urban settlements or bare land. The overestimation of estimated CO_2 over these areas is likely to be caused by atmospheric transportation that influences the spatial distribution of atmospheric CO_2 (Cao et al., 2017). Moreover, a large part of West Asia is covered by deserts, and these deserts observe a notably lower number of OCO-2 retrievals (Fig. 3a). The overestimation of the predicted CO_2 emissions over the largest desert of the region, the Rub' al Kahli, located in southern parts is likely to be caused by the uncertainties in the satellite-based XCO_2 anomalies, and these uncertainties are likely to be produced due to a lower number of OCO-2 retrievals. In addition, a previous study also indicated that the ACOS XCO_2 retrieval algorithm showed uncertainties over deserts (Bie et al., 2018). Similar to East Asia, the predicted CO_2 emissions over West Asia are also underestimated over areas that are covered by agriculture or vegetation, and this underestimation might be due to the presence of CO_2 uptake by the biosphere in the XCO_2 anomalies calculated using the satellite-based retrievals. The difference between the estimated values and the ODIAC CO_2 emissions ranged from -0.16×10^9 to 2.8×10^9 kg, and the magnitude of the difference between -1×10^9 and 1×10^9 kg accounted for 88 % of the total number of grid cell.

3.3 Correlation analysis between OCO-2 XCO_2 anomalies and ODIAC emissions

Figure 6 shows the correlation analysis between the ODIAC CO_2 emissions and the XCO_2 anomalies calculated using the OCO-2 retrievals over East and West Asia. Yang et al.

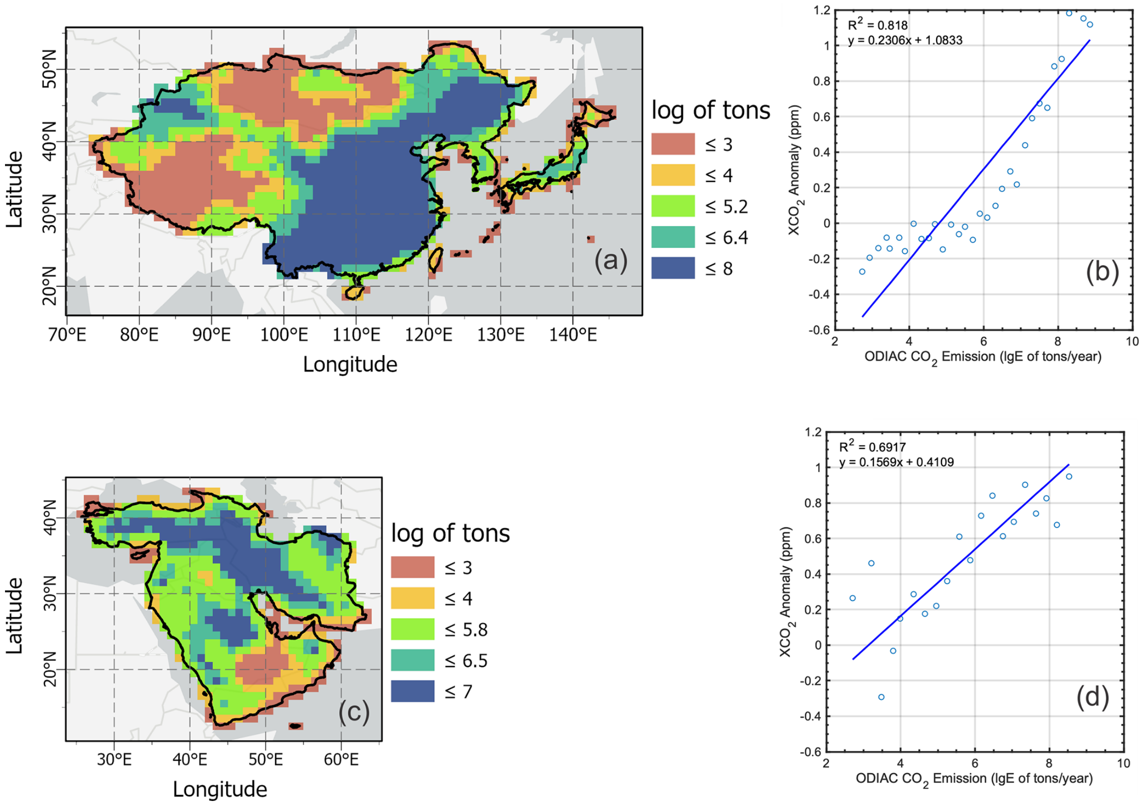

Figure 6. The spatial distribution of segmented ODIAC emissions, where the data are binned in $0.3\,\mathrm{t\,yr^{-1}}$ of lgE (logarithm of base 10) bins using the mean emission calculated from the annual emissions from 2015 to 2019 over **(a)** East Asia and **(c)** West Asia. The correlation between mean ODIAC CO_2 emissions and mean XCO_2 anomalies calculated from annual XCO_2 from 2015 to 2018 for **(b)** East Asia and **(d)** West Asia. (The base map was sourced from OpenStreetMap.)

(2019) found that the cluster of XCO_2 changes derived from satellite-based observations showed a better and more significant correlation with the CO_2 emissions relative to a single sounding of XCO_2, which might have been due to the fact that the atmospheric CO_2 measurement is an instantaneous snapshot of the realistic atmosphere (Liu et al., 2015). For the correlation analysis, we segmented the ODIAC emissions, which were binned every $0.3\,\mathrm{t\,yr^{-1}}$ of lgE (logarithm of base 10) using mean emissions calculated from annual emissions during 2015–2019, and then carried out an analysis between the mean of the emissions and the mean of the XCO_2 anomalies within the binned regions. The results showed a positive and significant correlation between the two datasets. Figure 6a and b show the spatial distribution of segmented ODIAC emissions over East Asia and the scatterplot between the mean of the emissions and the mean of the XCO_2 anomalies, respectively. The two datasets show a positive and significant correlation with a determined coefficient (R^2) of 0.81. The spatial distribution of segmented ODIAC emissions over West Asia and the scatterplot between the mean of the emissions and the mean of the XCO_2 anomalies for this region are shown in Fig. 6c and d, respectively. The two datasets showed a good correlation with a determined coefficient (R^2) of 0.60. Several studies have correlated satellite-based XCO_2 anomalies with CO_2 emissions (Fu et al., 2019; Shekhar et al., 2020). Yang et al. (2019) performed a correlation analysis between the GOSAT-based XCO_2 anomalies and the ODIAC CO_2 emissions over China and found a significant correlation with a determined coefficient (R^2) of 0.82 which increased up to 0.95 if the analysis was carried out with higher CO_2 emission values. In our study, the correlation between the CO_2 emissions and XCO_2 anomalies is relatively low for West Asia, which might be due to the uncertainties in the OCO-2 retrievals. A large part of West Asia is covered by deserts, and, as previously stated, Bie et al. (2018) reported that the ACOS XCO_2 retrieval algorithm showed uncertainties over deserts.

4 Summary and conclusions

In this study, anthropogenic CO_2 emissions were estimated using satellite datasets and employing a neural-network-based method. The study was carried out using ODIAC CO_2 emissions, OCO-2 XCO_2, and MODIS NPP datasets from 2015 to 2019. To remove the CO_2 seasonal variability and the large background concentration from the OCO-2 XCO_2

retrievals, XCO_2 anomalies were calculated for each year. A GRNN model was then built; XCO_2 anomalies, NPP, and CO_2 emissions from 2015 to 2018 were used as a training dataset; and, finally, CO_2 emissions were predicted for 2019 based on the NPP and XCO_2 anomalies calculated for the same year. The analyses were carried out separately over East and West Asia. The satellite-based estimated values and the ODIAC CO_2 emission datasets were compared, and both of the datasets showed good agreement in terms of spatial distribution. The estimated CO_2 emissions showed better results over East Asia compared with West Asia, which might be due to the uncertainties in the XCO_2 retrievals: previous studies have reported that the ACOS XCO_2 retrieval algorithm produced uncertainties over deserts. The predicted CO_2 emissions were generally overestimated, and this overestimation was larger over the areas that were closer to the high-density urban regions. The overestimations might be due to the nearby high-emission CO_2 sources that raised the XCO_2 concentration due to the effects of atmospheric transport. The satellite-based estimated CO_2 emissions were underestimated over some parts of the regions, mostly areas covered by agricultural land and vegetation; this was likely caused by the uncertainties in the calculated XCO_2 anomalies, and these uncertainties were produced due to the presence of the CO_2 uptake of the biosphere. We compared our results with a previous study carried out using a similar predictive model incorporating GOSAT XCO_2 retrievals (Yang et al., 2019). The referenced study generally underestimated the predicted CO_2 emissions, with larger differences relative to ODIAC CO_2 emissions, contradicting our results. Our study showed relatively better results, which might be due to several reasons: (i) we improved the predictive model with the addition of an NPP dataset, (ii) we incorporated OCO-2 XCO_2 retrievals that have a higher spatial resolution compared with the GOSAT XCO_2 retrievals, and (iii) we used a XCO_2 product processed using the latest version of the ACOS L2FP retrieval algorithm. The newer version of the algorithm has improved the quantity and the quality of the XCO_2 retrievals. Moreover, correlation analysis was also carried out between the ODIAC CO_2 emissions and the OCO-2 XCO_2 anomalies, and the results were significant with R^2 values of 0.81 and 0.60 over East and West Asia, respectively. These results were in agreement with the previous studies.

The results from our study suggest that CO_2 emissions can be estimated using observations obtained from CO_2 monitoring satellites. Currently, several satellites are orbiting the Earth and are dedicated to monitoring atmospheric CO_2. Joint utilization of the observations from the old and the latest satellites, such as OCO-3, GOSAT-2, and TanSAT, might reduce the spatiotemporal gaps and uncertainties. In future studies, we intend to improve the GRNN model via the addition of CO_2 uptake datasets and the joint utilization of multisensor data.

Data availability. The OCO-2 Level 2 XCO_2 product is available from https://doi.org/10.5067/E4E140XDMPO2 (OCO-2 Science Team et al., 2020), and the ODIAC CO_2 emission dataset is available from http://db.cger.nies.go.jp/dataset/ODIAC/ (CGER, 2021).

Author contributions. FM carried out the analysis under the supervision of LB, with input and support from QW, NY, MS, MB, RWA, and RI. FM wrote the original article with feedback from all the co-authors.

Competing interests. The contact author has declared that neither they nor their co-authors have any competing interests.

Disclaimer. Publisher's note: Copernicus Publications remains neutral with regard to jurisdictional claims in published maps and institutional affiliations.

Acknowledgements. The authors acknowledge the efforts of NASA with respect to providing the OCO-2 data products. The authors are also thankful to the National Institute of Environmental Studies (NIES) for providing the ODIAC CO_2 emission dataset. The lead author (Farhan Mustafa) is thankful to Thomas E. Taylor (Colorado State University, USA) for providing help with summarizing the evolution of the ACOS L2FP retrieval algorithm.

Financial support. This research has been supported by the National Natural Science Foundation of China (NSFC; grant no. 42175145) and the Shanghai Aerospace Science and Technology Innovation Fund (grant no. SAST 2019-045).

Review statement. This paper was edited by Dmitry Efremenko and reviewed by two anonymous referees.

References

Bao, Z., Zhang, X., Yue, T., Zhang, L., Wang, Z., Jiao, Y., Bai, W., and Meng, X.: Retrieval and Validation of XCO_2 from TanSat Target Mode Observations in Beijing, Remote Sens.-Basel, 12, 3063, https://doi.org/10.3390/rs12183063, 2020.

Bie, N., Lei, L., Zeng, Z., Cai, B., Yang, S., He, Z., Wu, C., and Nassar, R.: Regional uncertainty of GOSAT XCO_2 retrievals in China: quantification and attribution, Atmos. Meas. Tech., 11, 1251–1272, https://doi.org/10.5194/amt-11-1251-2018, 2018.

Boden, T. A., Andres, R. J., and Marland, G.: Global, regional, and national fossil-fuel CO_2 emissions (1751–2014) (v. 2017), Environmental System Science Data Infrastructure for a Virtual Ecosystem (ESS-DIVE) (United States), Carbon Dioxide Information Analysis Center (CDIAC), Oak Ridge National Laboratory (ORNL), Oak Ridge, TN, USA, 2017.

Bovensmann, H., Buchwitz, M., Burrows, J. P., Reuter, M., Krings, T., Gerilowski, K., Schneising, O., Heymann, J., Tretner, A., and Erzinger, J.: A remote sensing technique for global monitoring of power plant CO_2 emissions from space and related applications, Atmos. Meas. Tech., 3, 781–811, https://doi.org/10.5194/amt-3-781-2010, 2010.

Buchhorn, M., Lesiv, M., Tsendbazar, N.-E., Herold, M., Bertels, L., and Smets, B.: Copernicus Global Land Cover Layers—Collection 2, Remote Sens.-Basel, 12, 1044, https://doi.org/10.3390/rs12061044, 2020.

Cao, L., Chen, X., Zhang, C., Kurban, A., Yuan, X., Pan, T., and de Maeyer, P.: The Temporal and Spatial Distributions of the Near-Surface CO_2 Concentrations in Central Asia and Analysis of Their Controlling Factors, Atmosphere, 8, 85, https://doi.org/10.3390/atmos8050085, 2017.

Center for Global Environmental Research (CGER): ODIAC Fossil Fuel Emission Dataset, CGER [data set], available at: http://db.cger.nies.go.jp/dataset/ODIAC/, last access: 3 June 2021.

Chen, Z., Ye, X., and Huang, P.: Estimating Carbon Dioxide (CO_2) Emissions from Reservoirs Using Artificial Neural Networks, Water, 10, 26, https://doi.org/10.3390/w10010026, 2018.

Crisp, D.: Measuring atmospheric carbon dioxide from space with the Orbiting Carbon Observatory-2 (OCO-2), SPIE Optical Engineering + Applications, San Diego, California, United States, 8 September 2015, 960702, https://doi.org/10.1117/12.2187291, 2015.

Crisp, D., Fisher, B. M., O'Dell, C., Frankenberg, C., Basilio, R., Bösch, H., Brown, L. R., Castano, R., Connor, B., Deutscher, N. M., Eldering, A., Griffith, D., Gunson, M., Kuze, A., Mandrake, L., McDuffie, J., Messerschmidt, J., Miller, C. E., Morino, I., Natraj, V., Notholt, J., O'Brien, D. M., Oyafuso, F., Polonsky, I., Robinson, J., Salawitch, R., Sherlock, V., Smyth, M., Suto, H., Taylor, T. E., Thompson, D. R., Wennberg, P. O., Wunch, D., and Yung, Y. L.: The ACOS CO_2 retrieval algorithm – Part II: Global X_{CO_2} data characterization, Atmos. Meas. Tech., 5, 687–707, https://doi.org/10.5194/amt-5-687-2012, 2012.

Crisp, D., Pollock, H. R., Rosenberg, R., Chapsky, L., Lee, R. A. M., Oyafuso, F. A., Frankenberg, C., O'Dell, C. W., Bruegge, C. J., Doran, G. B., Eldering, A., Fisher, B. M., Fu, D., Gunson, M. R., Mandrake, L., Osterman, G. B., Schwandner, F. M., Sun, K., Taylor, T. E., Wennberg, P. O., and Wunch, D.: The on-orbit performance of the Orbiting Carbon Observatory-2 (OCO-2) instrument and its radiometrically calibrated products, Atmos. Meas. Tech., 10, 59–81, https://doi.org/10.5194/amt-10-59-2017, 2017.

Crowell, S., Baker, D., Schuh, A., Basu, S., Jacobson, A. R., Chevallier, F., Liu, J., Deng, F., Feng, L., McKain, K., Chatterjee, A., Miller, J. B., Stephens, B. B., Eldering, A., Crisp, D., Schimel, D., Nassar, R., O'Dell, C. W., Oda, T., Sweeney, C., Palmer, P. I., and Jones, D. B. A.: The 2015–2016 carbon cycle as seen from OCO-2 and the global in situ network, Atmos. Chem. Phys., 19, 9797–9831, https://doi.org/10.5194/acp-19-9797-2019, 2019.

EDGAR: Emission Database for Global Atmospheric Research (EDGAR v4.3.2), European Commission, 2017.

Fu, P., Xie, Y., Moore, C. E., Myint, S. W., and Bernacchi, C. J.: A Comparative Analysis of Anthropogenic CO_2 Emissions at City Level Using OCO-2 Observations: A Global Perspective, Earths Future, 7, 1058–1070, https://doi.org/10.1029/2019EF001282, 2019.

Guan, D., Liu, Z., Geng, Y., Lindner, S., and Hubacek, K.: The gigatonne gap in China's carbon dioxide inventories, Nat. Clim. Change, 2, 672–675, https://doi.org/10.1038/nclimate1560, 2012.

Gurney, K. R., Mendoza, D. L., Zhou, Y., Fischer, M. L., Miller, C. C., Geethakumar, S., and de la Rue du Can, S.: High Resolution Fossil Fuel Combustion CO_2 Emission Fluxes for the United States, Environ. Sci. Technol., 43, 5535–5541, https://doi.org/10.1021/es900806c, 2009.

Hakkarainen, J., Ialongo, I., and Tamminen, J.: Direct space-based observations of anthropogenic CO_2 emission areas from OCO-2, Geophys. Res. Lett., 43, 11400–11406, https://doi.org/10.1002/2016GL070885, 2016.

Hakkarainen, J., Ialongo, I., Maksyutov, S., and Crisp, D.: Analysis of Four Years of Global XCO_2 Anomalies as Seen by Orbiting Carbon Observatory-2, Remote Sens.-Basel, 11, 850, https://doi.org/10.3390/rs11070850, 2019.

Hoegh-Guldberg, O., D. Jacob, M. Taylor, M. Bindi, S. Brown, I. Camilloni, A. Diedhiou, R. Djalante, K.L. Ebi, F. Engelbrecht, J.Guiot, Y. Hijioka, S. Mehrotra, A. Payne, S.I. Seneviratne, A. Thomas, R. Warren, and G. Zhou, 2018: Impacts of 1.5 °C Global Warming on Natural and Human Systems, in: Global Warming of 1.5 °C. An IPCC Special Report on the impacts of global warming of 1.5 °C above pre-industrial levels and related global greenhouse gas emission pathways, in the context of strengthening the global response to the threat of climate change, sustainable development, and efforts to eradicate poverty, edited by: Masson-Delmotte, V., Zhai, P., Pörtner, H.-O., Roberts, D., Skea, J., Shukla, P. R., Pirani, A., Moufouma-Okia, W., Péan, C., Pidcock, R., Connors, S., Matthews, J. B. R., Chen, Y., Zhou, X., Gomis, M. I., Lonnoy, E., Maycock, T., Tignor, M., and Waterfield, T., IPCC, in press, 2021.

Hong, X., Zhang, P., Bi, Y., Liu, C., Sun, Y., Wang, W., Chen, Z., Yin, H., Zhang, C., Tian, Y., and Liu, J.: Retrieval of Global Carbon Dioxide From TanSat Satellite and Comprehensive Validation With TCCON Measurements and Satellite Observations, IEEE T. Geosci. Remote, 1–16, https://doi.org/10.1109/TGRS.2021.3066623, 2021.

Horowitz, C. A.: Paris Agreement, Int. Leg. Mater., 55, 740–755, https://doi.org/10.1017/S0020782900004253, 2016.

Hutchins, M. G., Colby, J. D., Marland, G., and Marland, E.: A comparison of five high-resolution spatially-explicit, fossil-fuel, carbon dioxide emission inventories for the United States, Mitig. Adapt. Strat. Gl., 22, 947–972, https://doi.org/10.1007/s11027-016-9709-9, 2017.

Jalil, S. A.: Carbon Dioxide Emission in the Middle East and North African (MENA) Region: A Dynamic Panel Data Study, Journal of Emerging Economies and Islamic Research, 2, 5, https://doi.org/10.24191/jeeir.v2i3.9629, 2014.

Janssens-Maenhout, G., Crippa, M., Guizzardi, D., Dentener, F., Muntean, M., Pouliot, G., Keating, T., Zhang, Q., Kurokawa, J., Wankmüller, R., Denier van der Gon, H., Kuenen, J. J. P., Klimont, Z., Frost, G., Darras, S., Koffi, B., and Li, M.: HTAP_v2.2: a mosaic of regional and global emission grid maps for 2008 and 2010 to study hemispheric transport of air pollution, Atmos. Chem. Phys., 15, 11411–11432, https://doi.org/10.5194/acp-15-11411-2015, 2015.

Keppel-Aleks, G., Wennberg, P. O., O'Dell, C. W., and Wunch, D.: Towards constraints on fossil fuel emissions from total column carbon dioxide, Atmos. Chem. Phys., 13, 4349–4357, https://doi.org/10.5194/acp-13-4349-2013, 2013.

Kiel, M., O'Dell, C. W., Fisher, B., Eldering, A., Nassar, R., MacDonald, C. G., and Wennberg, P. O.: How bias correction goes wrong: measurement of X_{CO_2} affected by erroneous surface pressure estimates, Atmos. Meas. Tech., 12, 2241–2259, https://doi.org/10.5194/amt-12-2241-2019, 2019.

Kong, Y., Chen, B., and Measho, S.: Spatio-temporal consistency evaluation of XCO_2 retrievals from GOSAT and OCO-2 based on TCCON and model data for joint utilization in carbon cycle research, Atmosphere, 10, 1–23, https://doi.org/10.3390/atmos10070354, 2019.

Konovalov, I. B., Berezin, E. V., Ciais, P., Broquet, G., Zhuravlev, R. V., and Janssens-Maenhout, G.: Estimation of fossil-fuel CO_2 emissions using satellite measurements of "proxy" species, Atmos. Chem. Phys., 16, 13509–13540, https://doi.org/10.5194/acp-16-13509-2016, 2016.

Korsbakken, J. I., Peters, G. P., and Andrew, R. M.: Uncertainties around reductions in China's coal use and CO_2 emissions, Nat. Clim. Change, 6, 687–690, https://doi.org/10.1038/nclimate2963, 2016.

Kumar, K. R., Revadekar, J. V., and Tiwari, Y. K.: AIRS retrieved CO_2 and its association with climatic parameters over india during 2004-2011, Sci. Total Environ., 476–477, 79–89, https://doi.org/10.1016/j.scitotenv.2013.12.118, 2014.

Lamminpää, O., Hobbs, J., Brynjarsdóttir, J., Laine, M., Braverman, A., Lindqvist, H., and Tamminen, J.: Accelerated MCMC for Satellite-Based Measurements of Atmospheric CO_2, Remote Sens.-Basel, 11, 2061, https://doi.org/10.3390/rs11172061, 2019.

Lauvaux, T., Miles, N. L., Deng, A., Richardson, S. J., Cambaliza, M. O., Davis, K. J., Gaudet, B., Gurney, K. R., Huang, J., O'Keefe, D., Song, Y., Karion, A., Oda, T., Patarasuk, R., Razlivanov, I., Sarmiento, D., Shepson, P., Sweeney, C., Turnbull, J., and Wu, K.: High-resolution atmospheric inversion of urban CO_2 emissions during the dormant season of the Indianapolis Flux Experiment (INFLUX), J. Geophys. Res.-Atmos., 121, 5213–5236, https://doi.org/10.1002/2015JD024473, 2016.

Liu, D., Lei, L., Guo, L., and Zeng, Z.-C.: A Cluster of CO_2 Change Characteristics with GOSAT Observations for Viewing the Spatial Pattern of CO_2 Emission and Absorption, Atmosphere, 6, 1695–1713, https://doi.org/10.3390/atmos6111695, 2015.

Liu, Y., Wang, J., Yao, L., Chen, X., Cai, Z., Yang, D., Yin, Z., Gu, S., Tian, L., Lu, N., and Lyu, D.: The TanSat mission: preliminary global observations, Sci. Bull., 63, 1200–1207, https://doi.org/10.1016/j.scib.2018.08.004, 2018.

Maksyutov, S., Takagi, H., Valsala, V. K., Saito, M., Oda, T., Saeki, T., Belikov, D. A., Saito, R., Ito, A., Yoshida, Y., Morino, I., Uchino, O., Andres, R. J., and Yokota, T.: Regional CO_2 flux estimates for 2009–2010 based on GOSAT and ground-based CO_2 observations, Atmos. Chem. Phys., 13, 9351–9373, https://doi.org/10.5194/acp-13-9351-2013, 2013.

Matsunaga, T., Morino, I., Yoshida, Y., Saito, M., Noda, H., Ohyama, H., Niwa, Y., Yashiro, H., Kamei, A., Kawazoe, F., Saeki, T., Ishihara, Y., Imasu, R., Teruyuki, N., Nakajima, T. S. Y., Saitoh, N., and Hashimoto, M.: Early Results of GOSAT-2 Level 2 Products, in: AGU Fall Meeting Abstracts, December 2019, abstract #A52H-02, 2019.

Mustafa, F., Bu, L., Wang, Q., Ali, M. A., Bilal, M., Shahzaman, M., and Qiu, Z.: Multi-year comparison of CO_2 concentration from NOAA carbon tracker reanalysis model with data from GOSAT and OCO-2 over Asia, Remote Sens.-Basel, 12, 2498, https://doi.org/10.3390/RS12152498, 2020.

Mustafa, F., Bu, L., Wang, Q., Yao, N., Shahzaman, M., Bilal, M., Aslam, R. W., and Iqbal, R.: Neural Network Based Estimation of Regional Scale Anthropogenic CO_2 Emissions Using OCO-2 Dataset Over East and West Asia, Atmos. Meas. Tech. Discuss. [preprint], https://doi.org/10.5194/amt-2021-222, in review, 2021a.

Mustafa, F., Wang, H., Bu, L., Wang, Q., Shahzaman, M., Bilal, M., Zhou, M., Iqbal, R., Aslam, R. W., Ali, M. A., and Qiu, Z.: Validation of GOSAT and OCO-2 against In Situ Aircraft Measurements and Comparison with CarbonTracker and GEOS-Chem over Qinhuangdao, China, Remote Sens.-Basel, 13, 899, https://doi.org/10.3390/rs13050899, 2021b.

OCO-2 Science Team, Gunson, M., and Eldering, A.: OCO-2 Level 2 bias-corrected XCO2 and other select fields from the full-physics retrieval aggregated as daily files, Retrospective processing V10r, Greenbelt, MD, USA, Goddard Earth Sciences Data and Information Services Center (GES DISC) [data set], https://doi.org/10.5067/E4E140XDMPO2, 2020.

ODell, C., Eldering, A., Gunson, M., Crisp, D., Fisher, B., Kiel, M., Kuai, L., Laughner, J., Merrelli, A., Nelson, R., Osterman, G., Payne, V., Rosenberg, R., Taylor, T., Wennberg, P., Kulawik, S., Lindqvist, H., Miller, S., and Nassar, R.: Improvements in XCO2 accuracy from OCO-2 with the latest ACOS v10 product, EGU General Assembly 2021, online, 19–30 Apr 2021, EGU21-10484, https://doi.org/10.5194/egusphere-egu21-10484, 2021.

O'Dell, C. W., Connor, B., Bösch, H., O'Brien, D., Frankenberg, C., Castano, R., Christi, M., Eldering, D., Fisher, B., Gunson, M., McDuffie, J., Miller, C. E., Natraj, V., Oyafuso, F., Polonsky, I., Smyth, M., Taylor, T., Toon, G. C., Wennberg, P. O., and Wunch, D.: The ACOS CO_2 retrieval algorithm – Part 1: Description and validation against synthetic observations, Atmos. Meas. Tech., 5, 99–121, https://doi.org/10.5194/amt-5-99-2012, 2012.

O'Dell, C. W., Eldering, A., Wennberg, P. O., Crisp, D., Gunson, M. R., Fisher, B., Frankenberg, C., Kiel, M., Lindqvist, H., Mandrake, L., Merrelli, A., Natraj, V., Nelson, R. R., Osterman, G. B., Payne, V. H., Taylor, T. E., Wunch, D., Drouin, B. J., Oyafuso, F., Chang, A., McDuffie, J., Smyth, M., Baker, D. F., Basu, S., Chevallier, F., Crowell, S. M. R., Feng, L., Palmer, P. I., Dubey, M., García, O. E., Griffith, D. W. T., Hase, F., Iraci, L. T., Kivi, R., Morino, I., Notholt, J., Ohyama, H., Petri, C., Roehl, C. M., Sha, M. K., Strong, K., Sussmann, R., Te, Y., Uchino, O., and Velazco, V. A.: Improved retrievals of carbon dioxide from Orbiting Carbon Observatory-2 with the version 8 ACOS algorithm, Atmos. Meas. Tech., 11, 6539–6576, https://doi.org/10.5194/amt-11-6539-2018, 2018.

Oda, T.: ODIAC Fossil Fuel CO2 Emissions Dataset (ODIAC2020, ODIAC2019, ODIAC2018, ODIAC2017, ODIAC2016, ODIAC2015a, ODIAC2013a), National Institute for Environmental Studies, Japan [data set], https://doi.org/10.17595/20170411.001, 2015.

Oda, T., Maksyutov, S., and Andres, R. J.: The Open-source Data Inventory for Anthropogenic CO_2, version 2016 (ODIAC2016): a global monthly fossil fuel CO_2 gridded emissions data product for tracer transport simulations and surface flux inversions, Earth

Syst. Sci. Data, 10, 87–107, https://doi.org/10.5194/essd-10-87-2018, 2018.

Olivier, J. G. J., Van Aardenne, J. A., Dentener, F. J., Pagliari, V., Ganzeveld, L. N., and Peters, J. A. H. W.: Recent trends in global greenhouse gas emissions:regional trends 1970–2000 and spatial distributionof key sources in 2000, Environm. Sci., 2, 81–99, https://doi.org/10.1080/15693430500400345, 2005.

Peylin, P., Law, R. M., Gurney, K. R., Chevallier, F., Jacobson, A. R., Maki, T., Niwa, Y., Patra, P. K., Peters, W., Rayner, P. J., Rödenbeck, C., van der Laan-Luijkx, I. T., and Zhang, X.: Global atmospheric carbon budget: results from an ensemble of atmospheric CO_2 inversions, Biogeosciences, 10, 6699–6720, https://doi.org/10.5194/bg-10-6699-2013, 2013.

Rao, M.: Machine Learning in Estimating CO_2 Emissions from Electricity Generation, in: Uncertainty Management in Engineering – Topics in Pollution Prevention and Controls [Working Title], IntechOpen, https://doi.org/10.5772/intechopen.97452, 2021.

Rooki, R.: Application of general regression neural network (GRNN) for indirect measuring pressure loss of Herschel–Bulkley drilling fluids in oil drilling, Measurement, 85, 184–191, https://doi.org/10.1016/j.measurement.2016.02.037, 2016.

Shan, Y., Guan, D., Zheng, H., Ou, J., Li, Y., Meng, J., Mi, Z., Liu, Z., and Zhang, Q.: China CO_2 emission accounts 1997–2015, Sci. Data, 5, 170201, https://doi.org/10.1038/sdata.2017.201, 2018.

Shekhar, A., Chen, J., Paetzold, J. C., Dietrich, F., Zhao, X., Bhattacharjee, S., Ruisinger, V., and Wofsy, S. C.: Anthropogenic CO_2 emissions assessment of Nile Delta using XCO_2 and SIF data from OCO-2 satellite, Environ. Res. Lett., 15, 095010, https://doi.org/10.1088/1748-9326/ab9cfe, 2020.

Specht, D. F.: A general regression neural network, IEEE T. Neural Networ., 2, 568–576, https://doi.org/10.1109/72.97934, 1991.

Takagi, H., Saeki, T., Oda, T., Saito, M., Valsala, V., Belikov, D., Saito, R., Yoshida, Y., Morino, I., Uchino, O., Andres, R. J., Yokota, T., and Maksyutov, S.: On the Benefit of GOSAT Observations to the Estimation of Regional CO_2 Fluxes, SOLA, 7, 161–164, https://doi.org/10.2151/sola.2011-041, 2011.

Taylor, T. E., Eldering, A., Merrelli, A., Kiel, M., Somkuti, P., Cheng, C., Rosenberg, R., Fisher, B., Crisp, D., Basilio, R., Bennett, M., Cervantes, D., Chang, A., Dang, L., Frankenberg, C., Haemmerle, V. R., Keller, G. R., Kurosu, T., Laughner, J. L., Lee, R., Marchetti, Y., Nelson, R. R., O'Dell, C. W., Osterman, G., Pavlick, R., Roehl, C., Schneider, R., Spiers, G., To, C., Wells, C., Wennberg, P. O., Yelamanchili, A., and Yu, S.: OCO-3 early mission operations and initial (vEarly) XCO_2 and SIF retrievals, Remote Sen. Environ., 251, 112032, https://doi.org/10.1016/j.rse.2020.112032, 2020.

Taylor, T. E., O'Dell, C. W., Crisp, D., Kuze, A., Lindqvist, H., Wennberg, P. O., Chatterjee, A., Gunson, M., Eldering, A., Fisher, B., Kiel, M., Nelson, R. R., Merrelli, A., Osterman, G., Chevallier, F., Palmer, P. I., Feng, L., Deutscher, N. M., Dubey, M. K., Feist, D. G., Garcia, O. E., Griffith, D., Hase, F., Iraci, L. T., Kivi, R., Liu, C., De Mazière, M., Morino, I., Notholt, J., Oh, Y.-S., Ohyama, H., Pollard, D. F., Rettinger, M., Roehl, C. M., Schneider, M., Sha, M. K., Shiomi, K., Strong, K., Sussmann, R., Té, Y., Velazco, V. A., Vrekoussis, M., Warneke, T., and Wunch, D.: An eleven year record of XCO_2 estimates derived from GOSAT measurements using the NASA ACOS version 9 retrieval algorithm, Earth Syst. Sci. Data Discuss. [preprint], https://doi.org/10.5194/essd-2021-247, in review, 2021.

Wang, J. S., Oda, T., Kawa, S. R., Strode, S. A., Baker, D. F., Ott, L. E., and Pawson, S.: The impacts of fossil fuel emission uncertainties and accounting for 3-D chemical CO_2 production on inverse natural carbon flux estimates from satellite and in situ data, Environ. Res. Lett., 15, 085002, https://doi.org/10.1088/1748-9326/ab9795, 2020.

Wang, R., Tao, S., Ciais, P., Shen, H. Z., Huang, Y., Chen, H., Shen, G. F., Wang, B., Li, W., Zhang, Y. Y., Lu, Y., Zhu, D., Chen, Y. C., Liu, X. P., Wang, W. T., Wang, X. L., Liu, W. X., Li, B. G., and Piao, S. L.: High-resolution mapping of combustion processes and implications for CO_2 emissions, Atmos. Chem. Phys., 13, 5189–5203, https://doi.org/10.5194/acp-13-5189-2013, 2013.

Wunch, D., Wennberg, P. O., Osterman, G., Fisher, B., Naylor, B., Roehl, C. M., O'Dell, C., Mandrake, L., Viatte, C., Kiel, M., Griffith, D. W. T., Deutscher, N. M., Velazco, V. A., Notholt, J., Warneke, T., Petri, C., De Maziere, M., Sha, M. K., Sussmann, R., Rettinger, M., Pollard, D., Robinson, J., Morino, I., Uchino, O., Hase, F., Blumenstock, T., Feist, D. G., Arnold, S. G., Strong, K., Mendonca, J., Kivi, R., Heikkinen, P., Iraci, L., Podolske, J., Hillyard, P. W., Kawakami, S., Dubey, M. K., Parker, H. A., Sepulveda, E., García, O. E., Te, Y., Jeseck, P., Gunson, M. R., Crisp, D., and Eldering, A.: Comparisons of the Orbiting Carbon Observatory-2 (OCO-2) X_{CO_2} measurements with TCCON, Atmos. Meas. Tech., 10, 2209–2238, https://doi.org/10.5194/amt-10-2209-2017, 2017.

Yang, D., Liu, Y., Cai, Z., Chen, X., Yao, L., and Lu, D.: First Global Carbon Dioxide Maps Produced from TanSat Measurements, Adv. Atmos. Sci., 35, 621–623, https://doi.org/10.1007/s00376-018-7312-6, 2018.

Yang, S., Lei, L., Zeng, Z., He, Z., and Zhong, H.: An Assessment of Anthropogenic CO_2 Emissions by Satellite-Based Observations in China, Sensors-Basel, 19, 1118, https://doi.org/10.3390/s19051118, 2019.